Denis Le Bihan, MD, PhD • Eric Breton, MS • Denis Lallemand, MD
• Marie-Louise Aubin, MD • Jacqueline Vignaud, MD • Maurice Laval-Jeantet, MD

Separation of Diffusion and Perfusion in Intravoxel Incoherent Motion MR Imaging[1]

Intravoxel incoherent motion (IVIM) imaging is a method the authors developed to visualize microscopic motions of water. In biologic tissues, these motions include molecular diffusion and microcirculation of blood in the capillary network. IVIM images are quantified by an apparent diffusion coefficient (ADC), which integrates the effects of both diffusion and perfusion. The aim of this work was to demonstrate how much perfusion contributes to the ADC and to present a method for obtaining separate images of diffusion and perfusion. Images were obtained at 0.5 T with high-resolution multisection sequences and without the use of contrast material. Results in a phantom made of resin microspheres demonstrated the ability of the method to separately evaluate diffusion and perfusion. The method was then applied in patients with brain and bone tumors and brain ischemia. Clinical results showed significant promise of the method for tissue characterization by perfusion patterns and for functional studies in the evaluation of the microcirculation in physiologic and pathologic conditions, as, for instance, in brain ischemia.

Index terms: Brain, MR studies, 13.1214 • Blood vessels, MR studies, 9.1299 • Magnetic resonance (MR), contrast enhancement • Magnetic resonance (MR), physics • Magnetic resonance (MR), pulse sequences • Magnetic resonance (MR), tissue characterization

Radiology 1988; 168:497-505

INTRAVOXEL incoherent motion (IVIM) is a term that designates the microscopic translational motions that occur in each image voxel in magnetic resonance (MR) imaging (1). In biologic tissues, these motions include molecular diffusion of water and microcirculation of blood in the capillary network (perfusion). Molecular diffusion refers to physical properties of tissue that allow tissues to be characterized. Microcirculation of blood or perfusion can also be considered an incoherent motion due to the pseudorandom organization of the capillary network at the voxel level (Fig 1). Perfusion imaging has the potential of characterizing tissues by their perfusion patterns, but also permits functional studies.

IVIM imaging is a method we developed to quantitatively image these motions (1,2). IVIMs were quantified in each voxel on the basis of an apparent diffusion coefficient (ADC). The ADC was equal to the diffusion coefficient D when diffusion was the only type of motion present, as we demonstrated in phantoms (1,2). However, ADCs in vivo were often higher than expected (1). These high values have been ascribed to microcirculation of blood in capillaries. The purpose of this work is to demonstrate how perfusion contributes to the ADC and to show how it is possible to obtain pure and separate images of diffusion and perfusion with the IVIM imaging method and without the use of any contrast agent. The theoretic principles of the method are explained, and evidence from specially built phantoms is used to support the validity of those principles. Clinical applications are then described and assessed.

THEORETIC BACKGROUND

Effects of IVIM on the MR Spin-Echo Signal

In the presence of magnetic field gradients, displacement of spins during the echo time (TE) of a spin-echo (SE) sequence produces a phase shift of the transverse magnetization (Fig 2a).

If a given voxel contains spins with different velocity vectors (amplitude and/or direction) during TE, a distribution of phase shifts results (Fig 2b). This loss of phase coherence in the transverse magnetization at the voxel level produces a spin-echo amplitude attenuation B, in addition to that created by the spin-spin relaxation process, so that the echo signal amplitude S in the voxel is

$$S(\mathrm{TE}) = S(0) \cdot B \cdot \exp(-\mathrm{TE}/\mathrm{T2}), \quad (1)$$

where T2 is the spin-spin relaxation time. The average dephasing in the voxel may be zero in the case of pure incoherent motions or different from zero if a net flow is present through the voxel. The intravoxel incoherent motions are thus responsible for this signal amplitude attenuation B ($B \leq 1$), the degree of which depends on the intensity of the IVIMs in the voxel and on the magnetic field gradients present during the sequence. In standard MR imaging these gradients are usually not significant with respect to the IVIM effects and B is close to unity ($B \simeq 1$), that is, no attenuation occurs from IVIMs. However, a significant attenuation of the echo signal will result from IVIMs if gradient pulses are added in an MR imaging sequence.

Molecular Diffusion

The attenuation term B is well known in the case of the diffusion process (3,4):

$$B = \exp(-b \cdot D), \quad (2)$$

where D is the diffusion coefficient and b is a factor depending only on the gradient pulse sequence, the gradient factor being a function of the third power of

[1] From the Groupe de Biophysique, Ecole Polytechnique, Palaiseau, France (D.L.B.); the College d'Evaluation en Resonance Magnetique, Paris (D.L.B., D.L., M.L.A., J.V., M.L.J.); and Thomson-CGR, Buc, France (E.B.). From the 1986 and 1987 RSNA annual meetings. Received January 4, 1988; revision requested February 4; revision received February 22; accepted February 24. **Address reprint requests to** D.L.B., Diagnostic Radiology Department, National Institutes of Health, Bldg 10, Rm 1C660, Bethesda, MD 20892.

See also the editorial by Dixon (pp 566-567) in this issue.

gradient pulse duration and of the second power of gradient strength, as described in previous publications (1,2). Since diffusion is a pure incoherent motion, the average dephasing of the transverse magnetization remains zero.

The diffusion coefficient D is related to molecular mobility. By use of a statistical approach, the Brownian motion can be described by a series of molecular jumps. If $\bar{l}$ is the mean length of these jumps and $\bar{v}$ the mean molecular velocity, the resulting diffusion coefficient D can be ascribed:

$$D = l\bar{v}/6. \quad (3)$$

Typical values for $\bar{l}$ and $\bar{v}$ are about 10^{-10} m and several hundred meters per second, respectively.

For pure water at 40°C, $D = 2.5 \cdot 10^{-3}$ mm²/sec. In biologic tissues, diffusion coefficients are lower, due to viscosity and restricted diffusion effects, offering tissue characterization possibilities (1).

Microcirculation

If we consider now the fraction of water diffusing and flowing in the capillaries of a given voxel, the spin-echo amplitude attenuation B in the presence of field gradients will include an additional term F due to microcirculation, the value of which will depend on capillary geometry and blood velocity. Hence

$$B = \exp(-bD) \cdot F, \quad (4)$$

where F is less than or equal to 1. The value for the function F can be calculated on a statistical basis because of the high quantity of capillaries in a voxel (5,700 per cubic millimeter in the brain cortex [5]). Assuming that the capillary network can be modeled by a network made of straight capillary segments, the expression for F will depend on the mean length $\bar{l}$ of the segments, the mean velocity $\bar{v}$ of blood in capillaries, and the measurement time T (which is approximately the echo delay TE). Two extreme cases can then be distinguished (6) (Fig 3).

First model (Fig 3a).—When blood flow changes capillary segments several times during T, movement of water in the capillary network mimics the diffusion process, as in a random walk. The expression for F is thus

$$F = \exp(-bD^*), \quad (5)$$

where D^* is now a pseudodiffusion coefficient. The value for D^* can be approximated by equation (3), where $\bar{l}$ is now the mean capillary segment length and $\bar{v}$ the blood velocity. The literature (7) indicates that $\bar{l}$ and $\bar{v}$ are 57 μm and 2.1 mm/sec respectively, in the cat brain. We can thus expect a value for D^* as high as $2.0 \cdot 10^{-2}$ mm²/sec, which is about ten times greater than the diffusion coefficient D of water measured in biologic tissues (8). The echo

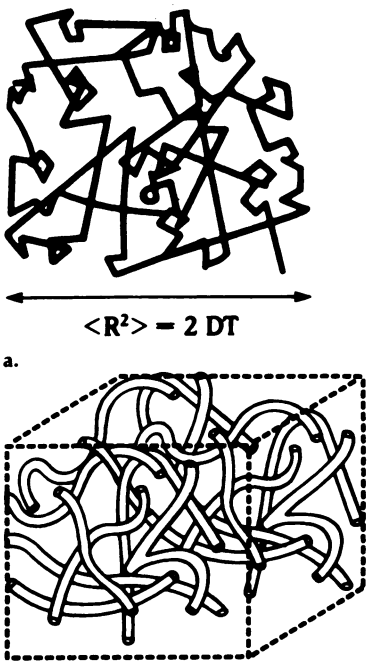

Figure 1. IVIMs designate the translational microscopic motions of water, which, in each voxel, involve a distribution of velocity directions and/or amplitudes. In biologic tissues, these motions are molecular diffusion and perfusion. **(a)** Molecular diffusion results from the random thermic molecular motion, called Brownian motion. The diffusion coefficient D characterizes the mobility of molecules—that is, their mean square displacement $\langle R^2 \rangle$ in a given time interval T. The diffusion coefficient of pure water at 40°C is $2.5 \cdot 10^{-3}$ mm²/sec, which corresponds to a mean displacement of 22 μm in 100 msec. **(b)** Perfusion results from blood microcirculation in the capillary network. Perfusion can be considered an incoherent motion due to the pseudorandom orientation of capillaries at the voxel level. Water flowing in capillaries involves only a fraction of the total water content of the voxel. This fractional volume is called here the perfusion factor f, typically a few percent.

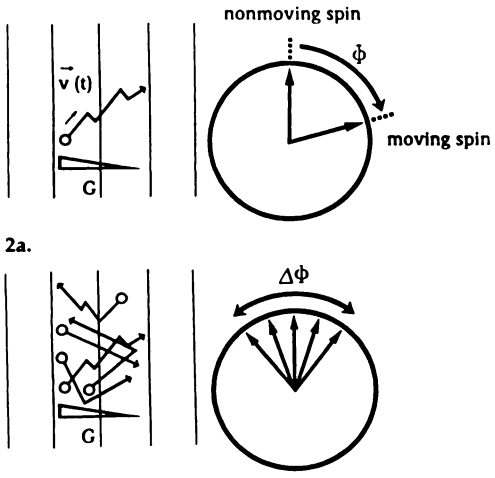

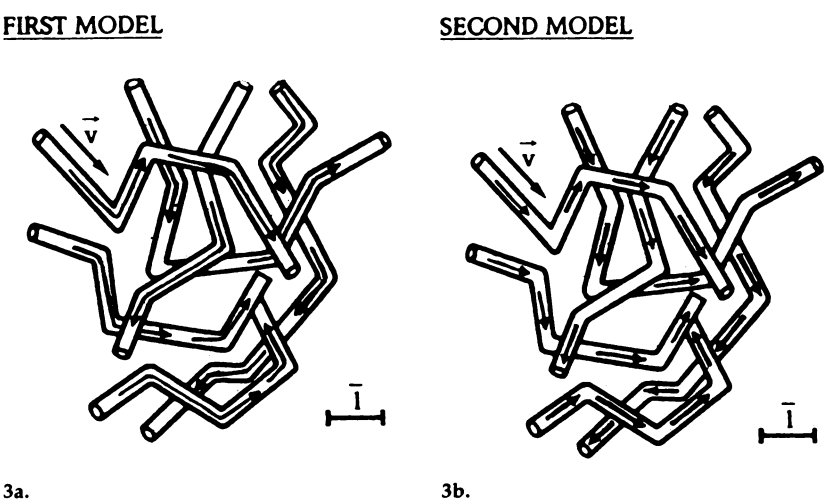

Figures 2, 3. **(2)** Effect of IVIM on the MR spin-echo signal. **(a)** Spin movements in the direction of a magnetic field gradient G produce phase shifts Φ of the transverse magnetization, as compared with nonmoving spins, due to changes in their precession frequency. **(b)** If spins present different movements in a given voxel, a distribution of phase shifts $\Delta\Phi$ results. This loss of coherence in transverse magnetization decreases the echo signal amplitude, as a function of the differences in spin motions and of the field gradients used. In the case of molecular diffusion, for instance, the echo attenuation is an exponential function of the diffusion coefficient D. **(3)** For capillary flow, the spin-echo amplitude attenuation F is a function of blood velocity $\bar{v}$ and capillary geometry. Assuming that the capillary network can be described by a succession of straight capillary segments, the mean length of which is $\bar{l}$, two situations can be considered to determine F. **(a)** If blood flow changes segments several times during the spin-echo sequence, movement of water in capillaries looks like a diffusion process—that is, a random walk—but at a more complex level. A pseudodiffusion coefficient D^* can be defined, the value of which would be determined by $\bar{l}$ and $\bar{v}$. **(b)** If blood flow does not change segment during the spin-echo sequence, the echo attenuation law becomes different. This situation occurs when the capillary segments are longer, the blood velocity is slower, or the spin-echo delay is shorter. Nevertheless, the echo attenuation F can be calculated by assuming a random orientation of the capillary segments at the voxel level. In both these cases, the echo attenuation due to perfusion is always greater than that due to diffusion, potentially allowing them to be separated on a quantitative basis.

attenuation resulting from perfusion will be thus always greater than that resulting from diffusion.

Second model (Fig 3b).—When blood flow is slower or the capillary segments are longer or the measurement time is shorter, blood flow does not change segment during T. The expression for F thus becomes different in this case, but may be evaluated by a simple approach (see Appendix), assuming pseudorandom orientations of the capillary segments. As for the diffusion or the pseudodiffusion approach, the average dephasing of the transverse magnetization remains zero in this case, and the effect of the capillary flow is a pure signal amplitude attenuation. If a net flow should be present in the voxel, probably related to small vessels rather than true capillaries, an average dephasing different from zero would be obtained, together with the signal amplitude attenuation. However, the IVIM technique takes care only of the signal attenuation. Other techniques, such as phase-imaging, might be able to display any dephasing. Furthermore, computer simulations showed that the first model (pseudodiffusion) applied when blood flow changed no more than four segments during the measurement time T. Such a situation often occurs when T is at least as long as 140 msec. These simulations also showed that, even in the case of the second model, the echo attenuation due to microcirculation was always greater than that due to diffusion.

This differential effect of diffusion and perfusion on the MR signal amplitude will allow them to be separated on a quantitative basis, as stated below.

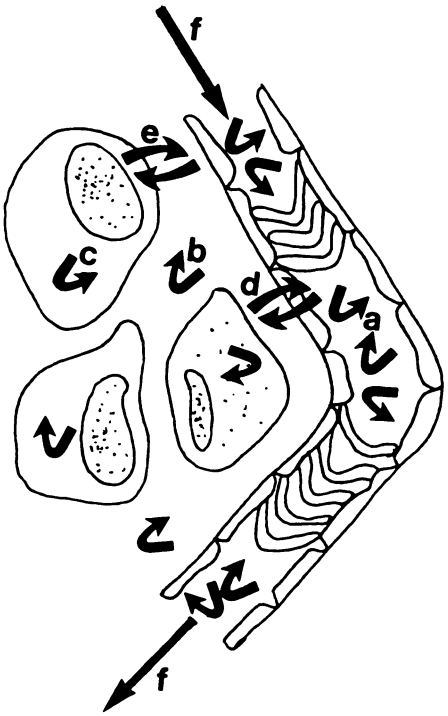

Figure 4. Model of biologic tissue. A tissue can be described by a volume fraction f of water flowing (f) and diffusing (a) in capillaries. This fraction involves only perfused capillaries, which are a part of total capillaries, depending on the current physiologic or pathologic situations. The rest of the voxel water, occupying a volume fraction $1 - f$, is involved in diffusion only. This volume fraction corresponds to extracellular (b) and intracellular (c) spaces. There are exchanges between those two compartments (e). In a simple approach, exchanges between water inside capillaries and outside capillaries (d) during the measurement time (100 msec) are neglected. Another assumption is that the diffusion coefficient in sectors a, b, and c is nearly the same.

Model of Biologic Tissue

In all cases, a biologic tissue includes a volume fraction f (typically a few percent) of water flowing in perfused capillaries, and a fraction $(1 - f)$ of static (diffusing only), intra- and extracellular water (Fig 4). In a simple approach, both components are assumed to have similar values for D and T2 and no net dephasing of their transverse magnetization. The echo attenuation in a single voxel can thus be written

$$S(\mathrm{TE}) = S(0) \cdot \exp(-\mathrm{TE}/\mathrm{T2}) \cdot \exp(-b \cdot D) \cdot [(1 - f) + fF]. \quad (6)$$

The purpose of IVIM imaging is to generate combined and/or separate images of the diffusion coefficient D and the perfusion factor f, regardless of capillary geometry or blood velocity. Perfusion images are thus images of the density of active capillaries, that is, those in which blood is flowing. Active capillaries represent only a fraction of total capillaries, as a function of physiologic states or pathologic conditions (57% in rat brain [5]).

PRINCIPLE OF DIFFUSION/ PERFUSION IMAGING

IVIM Imaging

IVIM images are generated from twin spin-echo sequences differently sensitized to these motions, as previously reported (1,2) (Fig 5). The first sequence (a) (Fig 5) is a standard spin-echo sequence in which the effects of IVIMs are negligible on the echo signals S_0. The second sequence (b) (Fig 5) contains additional gradient pulses to increase the effects of IVIMs on the echo signal S_1. The IVIM image is an image of the ADC obtained from such a pair of images—(a) and (b)—on a voxel-by-voxel basis:

$$\mathrm{ADC} = \mathrm{Log}(S_0/S_1)/(b_1 - b_0), \quad (7)$$

where b_1 and b_0 are the gradient factors of sequences S_1 and S_0. The use of the signal amplitude ratio S_0/S_1 allows the effects of spin density, T1, and T2 to be eliminated in the IVIM image when the same repetition time (TR) and TE are used in S_0 and S_1. The ADC becomes the diffusion coefficient D in a voxel if diffusion is the only type of motion present in the voxel. In the case of microcirculation, the ADC is greater than D. The contribution of the perfusion factor f to the ADC can be calculated by combining the relations defined in Equations (6) and (7).

A simple expression can be obtained under two hypotheses. First, the effects of diffusion and perfusion in S_0, the standard sequence, are negligible, as shown in previous publications (1,2), so that $\exp(-b_0 D) \simeq 1$ and $F_0 \simeq 1$; thus when Equation (6) is used, the echo attenuation in S_0 is

$$S(\mathrm{TE})_0 \simeq S(0) \cdot \exp(-\mathrm{TE}/\mathrm{T2}). \quad (8)$$

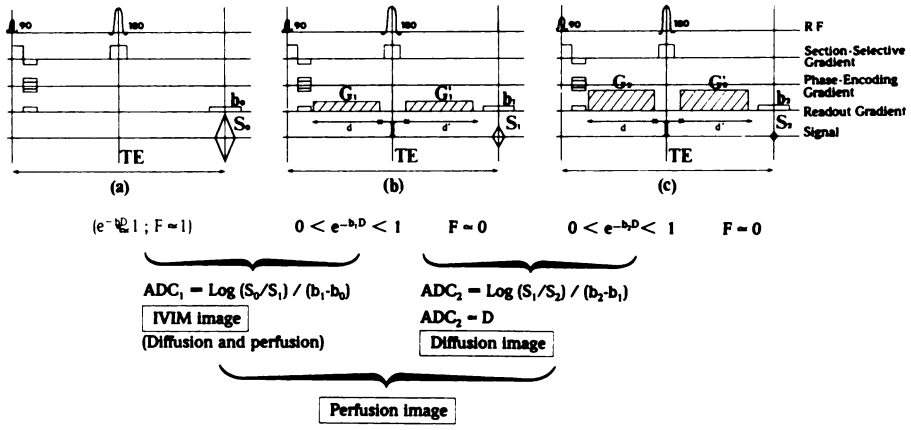

Figure 5. Separation of diffusion and perfusion. In order to generate separate images of diffusion and perfusion, three sequences are used. **(a)** Standard spin-echo sequence. Effects of diffusion and perfusion are negligible ($\exp[-b_0 \cdot D] \simeq 1$; $F_0 \simeq 1$). **(b)** Similar sequence, with additional gradient pulses (intensity G_1 and G_1'; duration d and d'). **(c)** Similar sequence with stronger additional gradient pulses (intensity G_2 and G_2'). The gradient strength in **b** and **c** is strong enough so that the contribution of microcirculation to the echo signals S_1 and S_2 is fully eliminated ($F \simeq 0$), while the contribution of diffusion is moderately reduced. This differential effect is possible because of the greater echo attenuation occurring from perfusion than from diffusion. Since the gradient strength in S_1 and S_2 is different, the sensitivity of these two sequences to diffusion differs. The IVIM image obtained from S_1 and S_2 is thus a pure diffusion image. By combining this diffusion image and the IVIM image obtained from S_0 and S_1, which depends on both diffusion and perfusion, a pure perfusion image can be extracted. b = gradient factor.

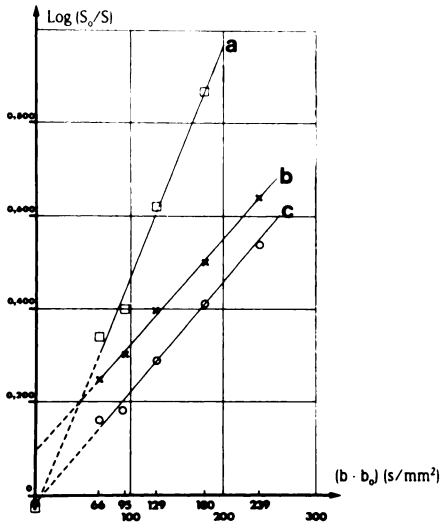

Figure 6. Phantom studies of (*a*) bottle filled with acetone, (*b*) chromatographic column packed with a resin made of microspheres in which a water flow was maintained, and (*c*) bottle filled with water. The logarithm of the echo attenuation S_0/S measured on images acquired with different extra-gradient strengths was plotted as a function of the gradient factor *b*. As expected from Equations (7) and (10), the plot was linear. The slope gave the diffusion coefficient *D*, whereas the intercept obtained by extrapolation was a function of the fractional volume occupied by the flowing component only. Quantitative results are shown in Table 2. Only *b* displays an intercept significantly different from zero. No significant difference was found for diffusion coefficients of water in the bottle (*c*) and in the chromatographic column (*b*).

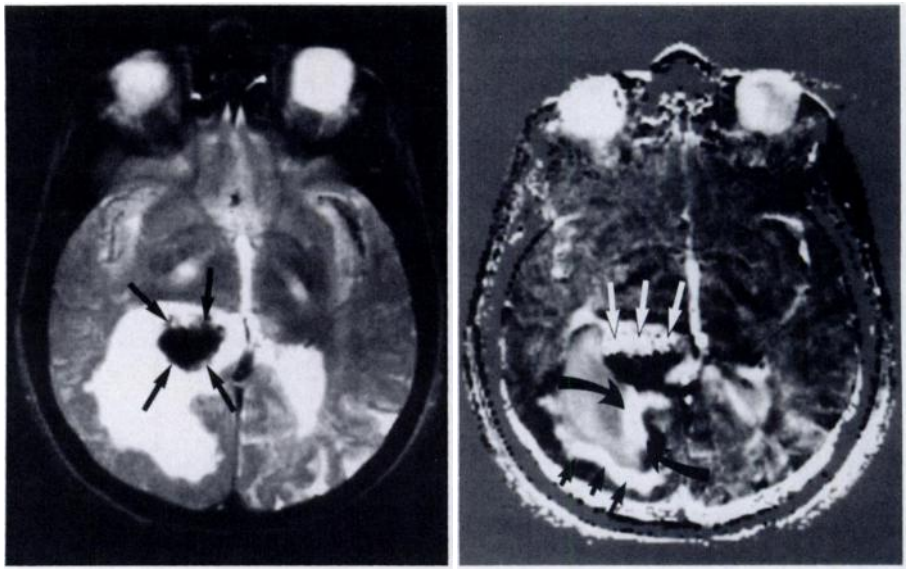

a. b.

Figure 7. Choroid plexus tumor. **(a)** T2-weighted transverse section (SE 1,000/140, 9-mm thickness, 256 × 256 resolution matrix). The tumor is clearly visible (arrows) inside the right occipital ventricular horn, which is dilated. Except for its location, no other information is provided regarding the tumor nature. **(b)** IVIM image of the same section. The anterior part of the tumor (straight white arrows) exhibits a very high ADC, which can indicate only a highly perfused, vascular tumor. The posterior part of the tumor is not visible, probably due to presence of calcifications. The size of the uncalcified part of the tumor appears greater in the IVIM image than expected from the T2 image. This case illustrates that information on perfusion usually obtained with contrast-enhanced CT can be obtained with MR imaging without using contrast agents. On the other hand, effects of the flow of cerebrospinal fluid (CSF) in IVIM imaging are clearly visible here. The hyperintense area near the posterior ventricular wall (short black arrows) could be ascribed to a laminar CSF flow, whereas the hyperintense area posterior to the tumor corresponds to a CSF jet (curved arrows). The value of the ADC in the eyes should be very carefully assessed because artifacts of eye motion may significantly decrease or increase the ADC, as in this image. Usually, the ADC in the eyes is close to that of static CSF.

Second, if the additional gradient pulses in sequences S_1 are long and/or strong enough so that $f \cdot F_1 \ll (1 - f)$, the contribution of the flowing component to the echo signal may be neglected ($F_1 \simeq 0$), whereas the contribution of diffusion is a moderate attenuation of the echo signal. This differential effect is possible according to the large differences in echo attenuation that result from perfusion and diffusion (Table 1). The echo attenuation in S_1 is thus

$$S(\mathrm{TE})_1 = S(0) \cdot \exp(-\mathrm{TE}/\mathrm{T2}) \cdot \exp(-b_1 \cdot D) \cdot (1 - f). \quad (9)$$

We obtain in these conditions for the ADC, from Equations (7)–(9),

$$\mathrm{ADC} = D + \mathrm{Log}[1/(1 - f)]/b_1. \quad (10)$$

Since in most cases $f \ll 1$, we finally obtain

$$\mathrm{ADC} \simeq D + (f/b_1). \quad (11)$$

The ADC appears to reflect both diffusion and perfusion. When typical values for *f* and b_1 are used—5% (5) and 100 sec/mm² (1), respectively—the relative contribution of the perfusion factor *f* to the ADC is about 25%. The ADC thus appears to be a sensitive index of perfusion. As shown in Equation (11), the ADC sensitivity to perfusion decreases when b_1 is high. The correct value for b_1 should be the minimal value compatible with the second hypothesis; that is, the contribution of perfusion to the echo signal S_1 is negligible. On the other hand, since *F* does not appear in Equation (11), capillary geometry and blood velocity need not be known. Furthermore, IVIM imaging requires only modified pulse sequences and not modified reconstruction software. Calculated IVIM images are produced in a similar way as calculated T2 images on many MR imaging systems.

Separation of Diffusion and Perfusion

According to the relation defined in Equation (10) or (11), a separate determination of *D* and *f* can be obtained from two IVIM images acquired with different gradient factors *b*. In practice, separate and quantitative images of diffusion and perfusion are calculated using a third sequence S_2 (6) (Fig 5). This sequence (*c*) (Fig 5) is identical to the S_1 sequence (*b*) (Fig 5), except that the additional gradient pulses are stronger so that the echo attenuation due to diffusion is greater in S_2 than in S_1. As the contribution of the flowing component is negligible in S_1 and S_2, the ADC image obtained from S_1 and S_2—that is, (*b*) and (*c*) (Fig 5)—is, under these conditions, a pure diffusion image (ADC = *D*).

By combining the first IVIM image obtained from S_0 and S_1—that is, (*a*) and (*b*) (Fig 5)—which depends on both diffusion and perfusion, and the pure diffusion image obtained from S_1 and S_2—that is (*b*) and (*c*) (Fig 5)—we extract a pure perfusion image from Equation (10):

$$f = 1 - \exp[-b_1 \cdot (\mathrm{ADC} - D)]. \quad (12)$$

Another way to get separate images of diffusion and perfusion would be to use the two IVIM images obtained from (*a*) and (*b*) and from (*a*) and (*c*), respectively, according to Equations (10) or (11), but this would require more calculation steps.

Capillary geometry also does not need to be known, since *F* is not used for any expression. Furthermore, with the IVIM technique perfusion images are obtained without the use of any contrast agent.

MATERIALS AND METHODS

Diffusion and perfusion images were obtained with a 0.5-T superconducting whole-body MR imager (Thomson-CGR, Buc, France). Images were acquired in a high-resolution (256 × 256 matrix) multisection mode. The method was initially

Table 1
Gradient Factors in IVIM Imaging

Sequence	Factor b (sec/mm^2)	$\exp(-b \cdot D)$	$F = \exp(-b \cdot D^*)$	Factor c (rd · sec/mm)	$F = \lvert\sin(c \cdot \bar{v})/(c \cdot \bar{v})\rvert$
First (S_0)	1.16	1.00	0.98	0.38	0.90
Second (S_1) (G_1 = 0.344 G/cm)	94.6	0.89	0.15	2.95	0.01
Third (S_2) (G_2 = 0.486 G/cm)	179.9	0.80	0.03	4.02	0.09

Note.—Diffusion: $D = 1.25 \cdot 10^{-3}$ mm^2/sec (water in biologic tissues, average value). Perfusion: $D^* = 2.0 \cdot 10^{-2}$ mm^2/sec (model 1); $\bar{v}$ = 2.1 mm/sec (model 2).

Table 2
Phantom Results

Fluid	"Perfusion Factor" f	Diffusion Coefficient D ($\times 10^{-3}$ mm^2/sec)
Acetone	−2.0% ± 2%	4.97 ± 0.20
Water (bottle)	−1.7% ± 2%	2.21 ± 0.10
Water (chromatographic column)	9.2% ± 2%	2.27 ± 0.10

Note.—McCall et al (9), and Cantor and Jonas (10) obtained a diffusion coefficient for acetone [D ($\times 10^{-3}$ mm^2/sec)] in the range of 4.5–4.8. James and McDonald (11) found one for water in the range of 2.25–2.51.

Table 3
Effect of Flow Rate on the Measured Perfusion Factor

Water Flow (mL/min)	ADC ($\times 10^{-3}$ mm^2/sec)	"Perfusion Factor" f
0	2.44 ± 0.10	0% ± 2%
3.7	2.82 ± 0.10	4% ± 2%
4.2	3.18 ± 0.10	7% ± 2%

Note.—The perfusion factor f is here the fractional volume of the column occupied by water flowing between microspheres.

used to evaluate both molecular diffusion and microcirculation on phantoms. It was then applied in patients.

Phantom Studies

A phantom was developed to demonstrate how microcirculation and diffusion contribute to the ADC in IVIM imaging and how these values can be separately determined. This phantom consisted of two tubes containing "static" (diffusing only) water and acetone at 25°C and a chromatographic column packed with a resin (Sephadex G100, Pharmacia, Uppsala, Sweden) in which water flow was maintained by gravity. The resin consisted of porous microspheres, 80 μm in diameter. Water inside the microspheres was diffusing only. Water in the interstitial volume between microspheres (volume fraction f) was assumed to flow in random orientations, as a model of microcirculation.

The section thickness was 9 mm and the spatial resolution was about 1 × 1 mm. The sequences were single-echo sequences with a TR of 1,000 msec and a TE of 140 msec (TR/TE = SE 1,000/140). Additional gradient pulses were applied along the readout gradient axis. The pulse duration was 40 msec with a 28-msec gap. Six values of gradient intensity were used: 0.280, 0.344, 0.408, 0.488, and 0.568 G/cm corresponding to values of 1.1, 67.0, 95.7, 130, 181, and 240 sec/mm^2, respectively, for the factor b.

The logarithm of the ratios of the echo signals of the standard sequence to the other sequences S_0/S was plotted as a function of $(b - b_0)$, according to Equations (7) and (10).

Human Studies

To demonstrate that the method could be used in clinical studies, we applied it to human subjects. A set of three to five sections was obtained for each acquisition. Image position and orientation were chosen according to lesion situation. The section thickness was 9 mm with a 9-mm intersection gap. The spatial resolution was 1.1 × 1.1 mm (28 × 28-cm field of view, 256 × 256 image matrix). Sequences used were SE 1,000/140 single-echo sequences (8 minutes, 32 seconds acquisition time). The corresponding gradient factors are given in Table 1. At the end of the acquisitions, both the standard images and the calculated images were displayed, that is, the IVIM images and/or the diffusion images and the perfusion images of each section.

Diagnosis had previously been established and results were correlated with findings at contrast-enhanced computed tomography (CT) and/or digital subtraction angiography.

We selected three cases to demonstrate the effects of perfusion in IVIM imaging; a choroid plexus tumor in a 35-year-old woman, a case of chronic brain ischemia in a 5-year-old boy with neonatal anoxia, and osteosarcoma of the distal extremity of the left femur in a 21-year-old woman. In this last, the possibility of separating diffusion and perfusion was also evaluated. Cardiac gating was used in all brain studies to eliminate brain pulsation artifacts but was not used in the study of the lower extremity.

RESULTS

Phantom Studies

As expected from Equations (7) and (10), the plot of $\text{Log}(S_0/S)$ as a function of $(b - b_0)$ for several values of b was linear (Fig 6):

$$\text{Log}(S_0/S) = (b - b_0) \cdot D + \text{Log}[1/(1 - f)]. \quad (13)$$

The slope gave the diffusion coefficient D, which was consistent with published data. The intercept gave the "perfusion factor" f, here the interstitial volume (Table 2). The value obtained here (10%) is, however, significantly lower than the expected value (32%), as determined by chromatography.

These differences have been ascribed to a too-low water flow through the column, since only the fraction of water flowing in the interstitial volume with a velocity higher than 800 μm/sec significantly decreases the echo signal in S_1 (with the gradient intensity used in our experiments). In order to validate this hypothesis, the water flow in the column was decreased (increasing it would have led to deterioration of the resin). The results in Table 3 verify this assumption: The measured "perfusion factor" f decreases with the water flow.

Table 4
Apparent Diffusion Coefficient in the Normal Brain (Frontal Area)

Tissue Type	S_0/S_1	ADC (10^{-3} mm²/sec)
Gray matter	1.21 ± 0.2	2.0 ± 0.1
White matter	1.17 ± 0.1	1.7 ± 0.1

Note.—The ADC was calculated with Equation (7). S_1 and S_0 refer to the spin-echo sequences with and without the additional gradient pulses (G = 0.344 G/cm; $b_1 - b_0$ = 93.5 sec/mm²).

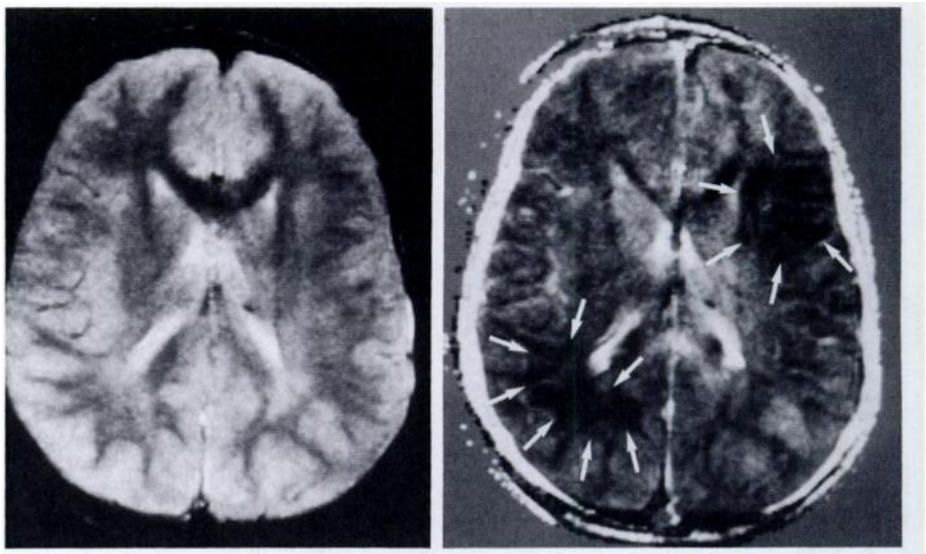

Figure 8. Chronic brain ischemia in a 5-year-old boy who presented with right motor deficiency and central visual troubles associated with neonatal anoxia. **(a)** T2-weighted transverse section (SE 1,000/120, 9-mm thickness, 256 × 256 resolution matrix). Except for the shape of the ventricular cavities no abnormalities are clearly demonstrated. **(b)** IVIM image of the same section. Two hypointense areas (arrows) are obviously displayed, one in the left sylvian area, one in the right parietooccipital area. The dark areas on the IVIM image correspond to areas of very low ADC and, since the tissue structure looked normal on the T2-weighted image, they can be related to a low-perfusion effect rather than a low-diffusion coefficient effect. These findings correlate well with the clinical findings. The low perfusion values could be a result of a partial deterioration of the active capillary bed. This case illustrates the aim of IVIM imaging to provide functional information. Reprinted, with permission, from reference 12.

Human Studies

Effects of perfusion in IVIM images.—In normal brain (Table 4), the ADC of gray matter was significantly higher than that of white matter ($2.0 \pm 0.1 \cdot 10^{-3}$ mm²/sec and $1.7 \pm 0.1 \cdot 10^{-3}$ mm²/sec, respectively), as previously reported (1). These differences correlate well with differences in perfusion between these two tissues, the factor f being about 5% and 2% for gray and white matter, respectively, in the rat brain (5).

The vascular nature of choroid plexus tumor (Fig 7) is well appreciated with contrast-enhanced CT. The IVIM image (Fig 7b) exhibits a high ADC in the tumor, demonstrating its vascular nature, whereas the standard T2-weighted image (Fig 7a) does not provide information on the nature of the tumor, except perhaps for its intraventricular location.

In cases of chronic ischemia (Fig 8) CT scans and conventional MR images (Fig 8a) only showed a slight abnormality in the left sylvian area. The IVIM image (Fig 8b) clearly exhibited two low-ADC areas, one in the left sylvian area, the other in the parietooccipital area. These findings correlated well with the clinical findings of visual and motor deficiency due to neonatal anoxia. These areas of low perfusion may be the result of a deterioration of the capillary bed.

Separation of diffusion and perfusion.—In a patient with osteosarcoma of femur (Fig 9), the significance of both the T2-weighted (Fig 9b) and the IVIM image (Fig 9e) was not clear in characterizing the tumor. The pure diffusion image (Fig 9f) showed higher diffusion coefficients in the posterior part of the tumor. This area probably corresponds to edema, in which water displacements are free. The perfusion image (Fig 9g) showed that perfusion is higher in the part of the tumor close to the bone, where capillary proliferation is the most active.

DISCUSSION

Technical Limitations

Motion artifacts.—Since the gradient moments used in the second and third sequences are strong in the readout gradient direction and the TE is long, the IVIM method is very sensitive to motion in this direction such as organ motion related to respiratory and pulsatile blood motion. Motion artifacts along the phase-encoding direction may result from random dephasings occurring at each cycle from motions along the IVIM-sensitized readout axis. Cardiac gating allows artifacts related to blood pulsations to be eliminated, by enabling the dephasings to be always the same at each cycle. Even for brain imaging, cardiac gating considerably increases the quality of IVIM images, and it should be used in clinical practice for studies of the brain or cervical spine. The direction of the phase-encoding gradient was chosen in brain studies to reject eye-motion artifacts outside the brain images. Cardiac gating was not necessary in extremity studies. Thoracoabdominal studies were not possible at the time of this work, due to motion artifacts and signal-to-noise ratio (S/N) considerations.

S/N.—Owing to the long TE used (TE = 140 msec in our experiments), which is necessary for long-duration gradient pulses, the T2 dependence of the source images is very strong. The S/N of the source images can be very low, for short T2. This situation occurs especially for thoracoabdominal tissues. One solution may be to shorten the TE, provided gradient strength does not get too large (the gradient factor b is a function of the third power of gradient duration and of the second power of gradient strength). The use of a strong gradient is possible only if gradient coils are well-compensated for the effect of eddy currents.

Another solution may be the use of stimulated echo sequences, as previously suggested (13). In fact, we recently developed a fast IVIM sequence using steady-state free precession (SSFP), which allows IVIM images to be obtained in a couple of minutes (14). This sequence would be less sensitive to motion artifacts and T2 effects.

Eddy currents.—As previously reported (1), the addition of strong gradient pulses on the readout gradient axis may be a source of artifacts on the IVIM images. These artifacts look like shift artifacts and are related to

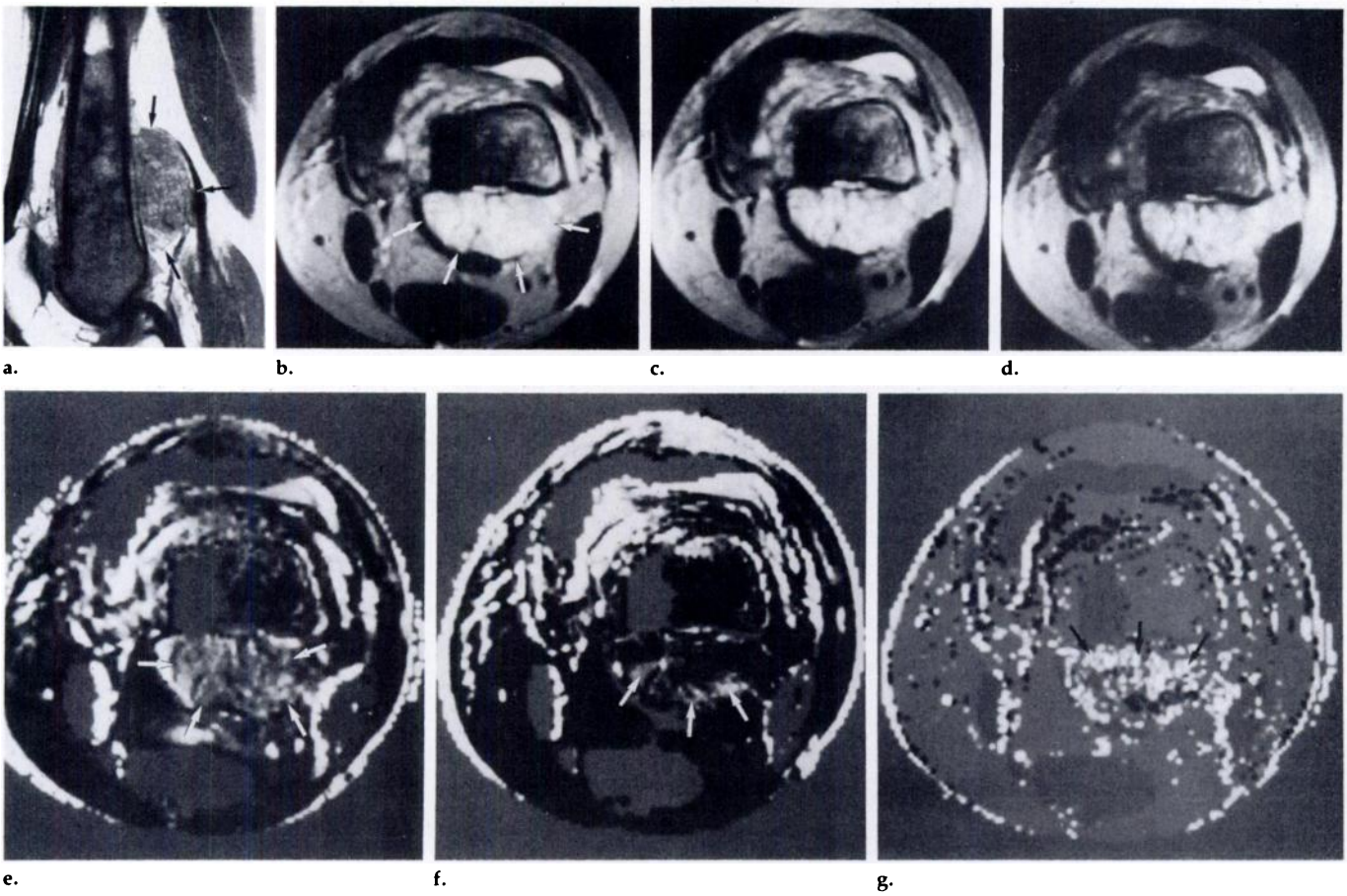

Figure 9. Separation of diffusion and perfusion images in 21-year-old woman with osteosarcoma of the distal extremity of the left femur. Images were obtained with a surface coil. **(a)** Sagittal section (SE 500/28, 7-mm thickness) shows extension of tumor into soft tissues (arrows). **(b-d)** Transverse sections (SE 1,000/140, 9-mm thickness). With sequence S_0 **(b)** extension of the tumor in soft tissues is visible, but its aspect is quite homogeneous (arrows). Tumor is only slightly less homogeneous with sequence S_1 ($G = 0.344$ G/cm) **(c)** and sequence S_2 ($G = 0.486$ G/cm) **(d). (e)** IVIM image of the same section calculated from S_0 and S_1. The tumor extension is also clearly visible in this image (arrows). However, precise identification of respective contributions to the ADC of diffusion and perfusion in this part of the tumor is difficult. **(f)** Pure diffusion image of the same section calculated from S_1 and S_2. The diffusion coefficient D is significantly higher in the posterior part of the tumor (arrows). This could be related to free displacement of water in edema, whereas in the tumor itself molecular displacement is limited by diffusion barriers (restricted diffusion). **(g)** Perfusion image calculated from images **e** and **f**. The perfusion factor f, or the capillary density, is obviously higher in the anterior part of the tumor (arrows), which is contiguous with bone, indicating that capillary proliferation is more intense in this portion of the tumor.

variations of the image size for each of the source images as a result of superimposition of the induced gradients with the readout gradient. The artifacts can be successfully eliminated by ad hoc timing and shaping of the gradient pulses inside the sequence and, if necessary, by postprocessing of the source images.

Models for Microcirculation

In microcirculation imaging it is assumed that blood water stays in the capillary network, at least during the measurement time (less than 140 msec in our experiments). Exchange between extra- and intracapillary water may be a source of mistakes in the evaluation of the fractional volume f. Haynor et al (15) have suggested the use of fluorinated blood substitutes to evaluate perfusion. Perfluorocarbons are assumed to remain in the bloodstream during the measurement time. However, the S/N in MR imaging of fluorine-19 is very low, due to low concentration, and there are large chemical shift effects. It could result in errors in measurements greater than that expected for the method proposed here when water exchange is neglected. Moreover, this exchange rate seems to be small (16), since the exchange flow is less than 0.1% of capillary flow.

Another assumption concerns the biphasic voxel model described: Both the flowing component (f) and the static component ($1 - f$) of water are assumed to have similar diffusion coefficients and T2 relaxation times. This assumption does not limit obtaining diffusion images since the flowing component is not included in the two source images (S_1) and (S_2). The apparent diffusion coefficient in a voxel is, in these conditions, the diffusion coefficient of water in the "static" component of the voxel. Only the perfusion factor f could be affected if this hypothesis is not true. When Equations (6) and (7) are used, it appears that only an estimation $\tilde{f}$ or the perfusion factor f is obtained, depending on the difference in T2 between the static and the flowing component. Differences in T2 may be significant if they are large enough. The effect of T2 could be limited by using shorter TEs with stronger gradient pulses or by using stimulated echoes.

The effect of blood pulsation during the cardiac cycle need not be considered when this approach is used, since it has no effect on the factor f. Furthermore, variations of blood velocity in the capillary network in relation to the pulsed blood pressure are known to be very small (17). On the other hand, dramatic changes can

be observed: Circulation in a given capillary can be stopped or inverted in direction within seconds (7). Microcirculation is thus better approached with the first model of microcirculation than with the second one. Cardiac gating may, however, be useful for eliminating motion artifacts, particularly for structures contiguous with blood vessels.

Comparison with Other Perfusion MR Imaging Methods

Only methods showing the capillary flow are assessed here. Several methods can be found in literature that demonstrate flow in small vessels (18) but not in the capillary bed.

Several studies have demonstrated the possibility of perfusion studies using contrast agents such as gadolinium complexes (19) or perfluorocarbons (15). Setting aside the potential toxic effects of these drugs, one drawback of applying contrast agents is that it is difficult to know precisely the quantity of agents fixed in biologic tissues, on which the MR signal amplitude can dramatically depend. When possible, pure physical and quantitative methods must be preferred.

An important point of the method proposed here is that perfusion imaging does not require any assumption on capillary geometry. Models proposed here were only to point out that the echo attenuation due to perfusion is always greater than that due to diffusion. If the expression for the function F is related to capillary geometry and blood velocity, this expression does not need to be known here, since only extreme values are used, that is, $F = 1$ or $F = 0$. This method thus appears more powerful than methods assuming even-echo rephasing (20). Rephasing of spins supposes that the capillary flow does not change in direction and/or amplitude during the TE of the spin-echo sequence. As stated above, in several tissues, such as brain, changes occurred in direction and amplitude of capillary flow (7). Furthermore, for phase images no net flow should occur from capillaries, meaning that phase images would be sensitive to blood flow in small vessels rather than in true capillaries.

Clinical Applications

IVIM imaging.—Clinical applications of IVIM imaging have previously been reported (1), and its potential use in the study of restricted diffusion effects and tissue perfusion—both for tissue characterization and functional studies—have been discussed. As regards diffusion and restricted diffusion, the measured diffusion coefficients in biologic tissues are lower than the diffusion coefficient of pure water ($2.5 \cdot 10^{-3}$ mm^2/sec at 40°C). This low value can be ascribed to the limitation of water displacements by microscopic obstacles in relation to physical tissue properties (8,21). These obstacles can be cellular membranes, as well as myelin fibers in brain white matter. On the other hand, other structures such as edema or cysts present diffusion coefficients close to that of pure water due to their free displacement of water. Edema and cysts can easily be recognized in IVIM images, even when T2-weighted images are confusing.

In these cases, separation of diffusion and perfusion need not be made, since no blood microcirculation effect hides the contribution of diffusion to the ADC in IVIM images. Separation of diffusion and perfusion is not necessary in cases in which the ADC is higher than the diffusion coefficient of pure water. Such a high value can only be the result of perfusion, as is demonstrated in this work.

IVIM images can be interpreted for perfusion in a similar way that contrast material–enhanced CT scans are: Areas of hyperintensity correspond to highly perfused areas. Tissue characterization can thus be done by studying perfusion patterns, that is, intensity and/or degree of homogeneity in perfusion.

Separation of diffusion and perfusion.—Because separation of diffusion and perfusion requires the use of a third sequence and is thus more costly in time, it should be used only when necessary—that is, when contribution of diffusion and perfusion in IVIM images is unclear, as in the case of the osteosarcoma presented here or when quantitative data are useful.

The fact that the capillary bed is demonstrated not through the uptake of a contrast medium, but directly, explains some observed differences between IVIM perfusion images and contrast-enhanced CT scans. Abnormal structures in brain, for instance, should be visible on IVIM perfusion images, whether the blood-brain barrier is disrupted or not, allowing both low-perfusion and high-perfusion lesions to be detected. Perfusion imaging has many other potential applications, including staging of malignant tumors or follow-up examination of patients treated with chemotherapy or radiation therapy. It may also provide functional imaging in a similar way that positron emission tomography does. In the case of chronic ischemia reported here, IVIM perfusion imaging already appears very promising, since the images show abnormalities not visible with either CT or standard MR imaging. Only active capillary beds are demonstrated—that is, beds in which blood is really flowing, depending on pathologic conditions or physiologic states, such as in brain cortical activation with sensorial stimulations. Work is now in progress to define areas in which the IVIM method is applicable for the detection of brain dysfunctions related to microcirculation abnormalities, such as stroke or arteriovenous malformations.

APPENDIX

The following explains how to determine the echo attenuation F for perfusion in the case of the second capillary geometry model.

The phase shift Φ of the transverse magnetization due to spin displacements during the TE of a spin-echo sequence is

$$\Phi = \gamma\left[\int_0^{TE/2} -\vec{v}\cdot\vec{G}\cdot t\cdot dt + \int_{TE/2}^{TE} \vec{v}\cdot\vec{G}\cdot t\cdot dt\right], \quad (A1)$$

where γ is the gyromagnetic ratio, $\vec{v}$ is the instantaneous velocity vector, and $\vec{G}$ is the instantaneous magnetic field gradient.

In the case of the second model of capillary geometry, blood flow does not change segment during TE and blood velocity is assumed to be constant, so that the velocity vector remains constant during TE. Considering the angle θ between the direction of a given capillary segment and the field gradient direction, the dephasing can be calculated from Equation (A1):

$$\Phi(v,\theta) = c\cdot v\cdot\cos\theta, \quad (A2)$$

where

$$c = \gamma\left[\int_0^{TE/2} -G\cdot t\cdot dt + \int_{TE/2}^{TE} G\cdot t\cdot dt\right]. \quad (A3)$$

When we take into account the distribution of orientations $\rho(\theta,\xi)$ of the capillary segments at the voxel level and the distribution of velocity $p(v)$, we obtain for the attenuation factor F:

$$F = \left|\int_0^{\infty}\int_0^{2\pi}\int_0^{\pi} e^{ic\cdot v\cdot\cos\theta}\cdot\rho(\theta,\xi)p(v)\sin\theta\,d\theta\,d\xi\,dv\right|. \quad (A4)$$

This expression for F simplifies for an iso-

tropic distribution of capillary segments and for a plug flow velocity v:

$$F = |\sin(c \cdot v)/(c \cdot v)|. \qquad (A5)$$

In our experiments, c was 2.95 rd·sec/mm and 4.02 rd·sec/mm in the second and third sequences, respectively (Table 1). The corresponding attenuation factors F were 0.01 and 0.09, respectively (v = 2.1 mm/sec). By comparison, the value of $\exp(-bD)$ for diffusion was 0.89 and 0.80, respectively. The echo attenuation due to perfusion was thus much larger for perfusion than for diffusion. ■

Acknowledgment: We are grateful to Maurice Gueron, PhD, for his constructive discussions and suggestions, particularly about the phantom experiments, and for his warm reception in his laboratory in Ecole Polytechnique.

References

1. Le Bihan D, Breton E, Lallemand D, Grenier P, Cabanis E, Laval-Jeantet M. MR imaging of intravoxel incoherent motions: application to diffusion and perfusion in neurologic disorders. Radiology 1986; 161:401-407.
2. Le Bihan D, Breton E. Imagerie de diffusion in-vivo par resonance magnetique. CR Acad Sci [II] 1985; 15:1109-1112.
3. Hahn EL. Spin echoes. Phys Rev 1950; 80:580-594.
4. Carr HY, Purcell EM. Effects of diffusion on free precession in nuclear magnetic resonance experiments. Phys Rev 1954; 94:630-635.
5. Weiss HR, Buchweitz E, Murtha TJ, Auletta M. Quantitative regional determination of morphometric indices of the total and perfused capillary network in the rat brain. Circ Res 1982; 51:494-503.
6. Le Bihan D, Breton E, Gueron M. Separation of perfusion and diffusion in intravoxel incoherent motion (IVIM) imaging. In: Book of abstracts: Society of Magnetic Resonance in Medicine 1986. Vol WIP. Berkeley, Calif: Society of Magnetic Resonance in Medicine, 1986; 7-8.
7. Pavlik G, Rackl A, Bing RJ. Quantitative capillary topography and blood flow in the cerebral cortex of cats: an in-vivo microscopic study. Brain Res 1981; 208:35-58.
8. Cooper LC, Chang DB, Young AC, Martin CJ, Johnson B. Restricted diffusion in biophysical systems. Biophysiol J 1974; 14:161-177.
9. McCall DW, Douglass DC, Anderson EW. Diffusion in liquids. J Chem Phys 1959; 31:1555-1557.
10. Cantor DM, Jonas J. Automated measurement of self-diffusion coefficients by the spin-echo method. J Magn Reson 1977; 28:157-162.
11. James TL, McDonald GG. Measurement of the self-diffusion coefficient of each component in a complex system using pulsed-gradient Fourier transform NMR. J Magn Reson 1973; 11:58-61.
12. Le Bihan D, Breton E, Lallemand D, Aubin ML, Vignaud J, Laval-Jeantet M. Contribution of intravoxel incoherent motion (IVIM) imaging to neuroradiology. J Neuroradiol 1987; 14:295-312.
13. Merboldt KD, Hanicke W, Frahm J. Self-diffusion NMR imaging using stimulated echoes. J Magn Reson 1985; 64:479-486.
14. Le Bihan D. Intravoxel incoherent motion imaging using steady-state free-precession. Magn Reson Med (in press).
15. Haynor DR, Richards TL, See W, Wesbey G. Perfluorocarbons for detection of tissue perfusion: use of pulsed field gradients. In: Book of abstracts: Society of Magnetic Resonance in Medicine 1986. Vol 2. Berkeley, Calif: Society of Magnetic Resonance in Medicine, 1986; 325-326.
16. Intaglietta M. Transcapillary exchange of fluid in single microvessels. In: Kaley G, Altura BM, eds. Microcirculation. Vol 1. Baltimore: University Park, 1977; 197-249.
17. Gross JF. The significance of pulsatile microhemodynamics. In: Kaley G, Altura BM, eds. Microcirculation. Vol I. Baltimore: University Park, 1977; 365-390.
18. Mueller E, Deimling M, Rheinardt ER. Quantification of pulsatile flow in MRI by an analysis of T2 changes in ECG-gated multiecho experiments. Magn Reson Med 1986; 3:331-335.
19. Runge VM, Clanton JA, Price AC, et al. The use of Gd DTPA as a perfusion agent and marker of blood-brain barrier disruption. Magn Reson Imaging 1985; 3:43-55.
20. Ahn CB, Lee SY, Nalcioglu O, Cho ZH. Capillary density imaging with NMR. In: Book of abstracts: Society of Magnetic Resonance in Medicine 1986. Vol 1. Berkeley, Calif: Society of Magnetic Resonance in Medicine, 1986; 102-103.
21. Stejskal EO. Use of spin-echoes in a pulsed magnetic field gradient to study anisotropic, restricted diffusion and flow. J Chem Phys 1965; 43:3597-3606.